Dynamical Criteria for Cs Ion Insertion and Adsorption at Cap and Stem of Carbon Nanotubes: Ab Initio Study and Comparison with Experiment

ARTICLE *in* THE JOURNAL OF PHYSICAL CHEMISTRY B · SEPTEMBER 2004

Impact Factor: 3.3 · DOI: 10.1021/jp0481557

BATCH: jp10b75 USER: dgw69 DIV: @xyv04/data1/CLS_pj/GRP_jp/JOB_i41/DIV_jp0481557 DATE: September 2, 2004

Dynamical Criteria for Cs Ion Insertion and Adsorption at Cap and Stem of Carbon Nanotubes: Ab Initio Study and Comparison with Experiment

Mohammad Khazaei,*,† Amir A. Farajian,† Goo-Hwan Jeong,‡ Hiroshi Mizuseki,† Takamichi Hirata,‡ Rikizo Hatakeyama,‡ and Yoshiyuki Kawazoe†

Institute for Materials Research, Tohoku University, Sendai 980-8577, Japan, and Department of Electronic Engineering, Tohoku University, Sendai 980-8579, Japan

Received: April 28, 2004; In Final Form: July 31, 2004

Unlike lighter alkali metals, cesium is not inserted into carbon nanotubes straightforwardly. To clarify Cs^+ insertion and adsorption processes in recent experiments, the Cs^+ is shot toward the cap and stem of (5,5) and (10,10) armchair nanotubes by performing ab initio molecular dynamics simulations. Considering three relevant factors of collision, i.e., the impact position, impact angle, and the kinetic energy of dopant, we observe that the Cs^+ with kinetic energy 50 eV is adsorbed on the surface of the nanotube irrespective of the impact angle and impact position. The Cs^+ with kinetic energy 100 eV can make a hole on the surface and be encapsulated, or trapped in the middle of the created hole, if the collision route is aiming toward the nanotube stem. If the route is aiming away from the nanotube stem, the Cs^+ will tear the nanotube's surface and will be scattered off. This makes it possible for other Cs ions to get encapsulated via the torn region. The Cs ions whose energies are 150 eV and aim toward the nanotube stem get encapsulated with minimal deformation of the collision region. The simulation results are supported by Raman scattering spectroscopy experiments and are instructive in doped-nanotube applications such as flat panel displays and nanoelectronic devices.

1. Introduction

Recently, there have been many advances in controlling the growth of long nanotubes in arbitrary orientations. This can be considered the start signal for a new generation of nanoscale devices based on the nanotubes. In this area, flat panel displays are closest to commercial application. Several groups have already fabricated prototypes of such displays.[1−3] The results indicate that among various types of nanotubes capped nanotubes are stable against applying electric field. It is theoretically shown that the binding energy of capped carbon nanotubes increases under an electric field.[4,5] Other investigations have indicated that adsorption of elements and molecules on the surface of nanotube can change the resistivity, threshold voltage, transport, and field-emission current drastically.[6−8] Alkali metals, for example, donate their valence electron to the nanotube. The resultant positive ion induces its image on surface of the nanotube and produces a dipole. The resulting dipole configuration reduces the surface barrier for the field emission.[9] For H_2O adsorption, on the other hand, charge transfers from the nanotube to H_2O, thereby the density of electrons in nanotube decreases which results in a decrease of transport current.[10] Available experimental data show the significance of the tunneling through single adatoms on the cathode surface in field emission. The peaks of experimental field emission electron spectra from nanoprotrusion tips, ending in a single atom adsorbed on the surface, suggest that the tunneling occurs only through localized states at the topmost atom.[11]

Considering these issues about the field emission from nanotube, doped, capped nanotubes are good candidate for flat panel displays. Among adsorbate elements, alkali metals, especially Cs, are considered to be the best dopants for achieving the above-mentioned goals. Cs is one of the heaviest elements in the periodic table and can donate its electron easier than other alkali metals.[12−14] Cs adsorption can also make a very sharp point on the surface that is convenient for emission. In addition to the role of adsorption of foreign dopants in field emission, encapsulated dopants are also expected to be useful in nanoelectronic applications, e.g., nanodiodes.[15,16]

There are some reports on intercalation of alkali metals in nanotube bundles by vapor deposition.[12,14,17,18] Moreover, experimental encapsulation of Cs ions in single wall nanotube via plasma ion irradiation is reported recently. The formation of an actual nanojunction is confirmed in these experiments,[19,20] where the Cs ions accelerate under the exerted electric field toward a substrate covered with dispersed nanotubes. On the substrate, the nanotubes have been distributed randomly[21] so the Cs ions collide with the capped nanotubes at different positions/angles.

A theoretical explanation of encapsulation of light alkali metals in nanotubes is more or less clear. Alkali metals that are shot with suitable kinetic energy toward hexagon rings of the nanotube widen the rings and enter. After encapsulation, the carbon ring restores its initial configuration.[22] But in the case of Cs with big radius the encapsulation procedure is not clear. There are also several theoretical studies on the insertion or adsorption of H_2, O_2, and H_2O.[6,8,23,24] To the best of our knowledge there is no theoretical report about the insertion or adsorption of Cs or Cs^+. The main propose of the present work

* Corresponding author. E-mail: khazaei@imr.edu.
† Institute for Materials Research.
‡ Department of Electronic Engineering.

10.1021/jp0481557 CCC: $25.00
Published on Web 00/00/0000 PAGE EST: 6.2

TABLE 1: Definitions of Different Impact Routes

route	target	direction
S1	a carbon atom	perpendicular to the tube axis along radial direction in the corresponding cylindrical coordinates
S2	a carbon atom	perpendicular to the tube axis and tangent to the surface of the nanotube
S3	the center of a bond	perpendicular to the tube axis along radial direction
S4	the center of a hexagon ring	perpendicular to the tube axis along radial direction
C1	the center of the pentagon ring at the tip of the cap	parallel to the tube axis or normal to the ring surface
C2	the center of a pentagon ring at the tip near the stem	normal to the ring surface
C3	a hexagon ring at the cap near the stem	normal to the ring surface
C4	a carbon atom which belongs to the pentagon ring at the tip of the cap	perpendicular to the tube axis

is to simulate the adsorption and insertion of Cs^+ at different positions, angles, and kinetic energies in capped nanotubes by ab initio molecular dynamics (MD).

2. Calculation Method

Our calculation is ab initio based on generalized gradient approximation (GGA) in density functional theory. The exchange-correlation functional of GGA is parametrized by the Perdew−Burke−Ernzerhof approach.[25] The core electrons are represented by improved Troullier−Martins pseudopotentials.[26] Valence electrons (2s and 2p for carbon and 6s, 6p, and 5d for Cs) are described by numerical atomic orbital basis sets.[27] The calculations are performed using SIESTA code.[28−30] The basis set is split valence double-ζ plus polarization orbitals.[31] Direct diagonalization of Kohn−Sham Hamiltonian is used for calculating the electronic structure. The conjugate gradient method is used for optimization of structures. Our calculations are microcanonical (without energy dispersion). We do not impose any artificial temperature or velocity control. We check the reliability of our method by comparing our results against the available experimental and theoretical data in the following cases: Cs_2 and Cs_2^+ dimer bond lengths,[32] different stable CsC_9^- isomers,[33] and the activation energy (sometimes called the corrugation energy) for Cs intercalated graphite.[34] Comparing our results with the available data results in good agreements. We choose the mesh cutoff and time-step length to be 135 Ry and 1.0 fs, respectively, after checking their quality.

Our calculations have been done using four different initial structures. The first two structures indicate the stems (main body) of (5,5) and (10,10) armchair nanotubes that contain 160 and 320 carbon atoms, respectively. The (10,10) tube is chosen for having the same diameter as that of the tubes used in experiments, and the (5,5) tube serves for comparison. The other two structures indicate capped (5,5) and (10,10) armchair nanotubes that include half of C_{60} and C_{240} fullerenes for the caps, respectively. The latter two structures contain 110 and 290 carbon atoms. In our simulations, we keep two ending rings of the stem and capped structures fixed in order to mimic the presence of long nanotubes in actual experiments and reduce the ending C−C bond lengths to 1.24 Å. All the other carbon atoms are relaxed until the maximum force on unconstrained atoms is less than 0.06 eV/Å. After relaxation, the observed C−C bond lengths for the capped structures are between 1.38 and 1.47 Å. For the stems, they are between 1.40 and 1.45 Å. This is in very good agreement with a pervious ab initio calculation,[30] where the reported bond lengths for the stem are between 1.42 and 1.45 Å.

3. Collision Routes

To simulate the collision of Cs ions with the stem and capped structures, we consider different collision routes. This is in accordance with the actual experimental situation[19,20] where the substrate is covered with randomly oriented nanotubes. We divide the routes into two main groups: The routes whose targets lie on the stem structures will be indicated by the symbol "**S**", and the routes whose targets lie on the capped structures will be indicated by "**C**". Different routes are defined in Table 1 and depicted in Figure 1. Since our calculations are done on both (5,5) and (10,10) nanotubes, we use abbreviations like **C4**(10,10), which means that the Cs^+ is shot along the route 4 toward (10,10) capped nanotube, and **S3**(5,5), which means that the Cs^+ is shot along the route **S3** toward the stem of the (5,5) nanotube. The initial distance between the Cs^+ and the target along the **C** and **S** routes is 4.0 Å for both (5,5) and (10,10) except for **C4**(10,10) and **S2**(10,10), for which the initial distance is 5.0 Å. We select these distances so as to make the force exerted on the Cs^+ negligible at the start of the simulation.

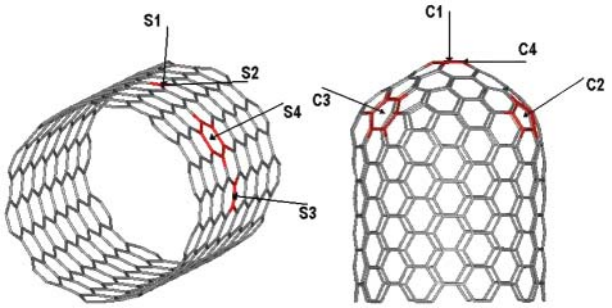

Figure 1. Different impact routes considered in present study.

4. Results and Discussion

As a result of Cs^+ collision, part of the Cs^+ kinetic energy is transferred to the carbon lattice. If the carbon atoms gain enough kinetic energy, they can break the bonds with neighboring carbon atoms. Otherwise, the carbon atoms will just oscillate and no bond breaking is observed. Bellow, we consider the effects of three relevant factors on the outcome of the impact. These relevant factors are the kinetic energy of Cs^+, the impact position, and the impact angle. We investigate three typical initial kinetic energies: 50, 100, and 150 eV. In the recent experiments[19,20] the average of Cs^+ kinetic energy is around 100 eV. We therefore explain the Cs^+ collision at 100 eV at full length. As the probability of Cs^+ collision with the inner area of hexagon rings is more than the collision probability for other positions, e.g., pentagon areas, atoms, and bonds, we describe the elongation and contraction of the bonds and effective potential for the route **C3** in (10,10) nanotube, i.e, **C3**(10,10), in detail, and mention the results of the other routes briefly. We call all the carbon atoms that belong to the target hexagon ring "α" and all the carbon atoms that do not belong to the hexagon ring and are nearest neighbors to the hexagon

BATCH: jp10b75 USER: dgw69 DIV: @xyv04/data1/CLS_pj/GRP_jp/JOB_i41/DIV_jp0481557 DATE: September 2, 2004

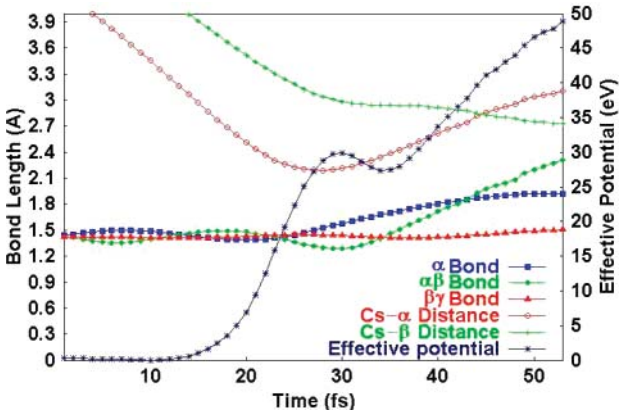

Figure 2. Effective potential and the averages of α, $\alpha\beta$, and $\beta\gamma$ bonds as well as Cs−α and Cs−β distances vs time along the route **C3**(10,10). The initial kinetic energy of Cs^+ is 100 eV.

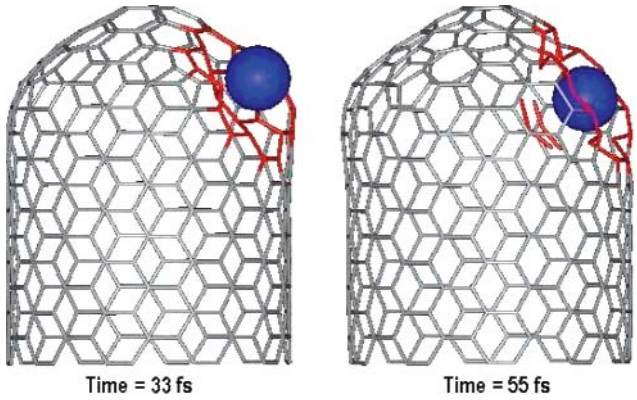

Figure 3. Snapshots of the Cs^+ insertion with initial kinetic energy 100 eV along the route **C3**(10,10) at 33 and 55 fs. Cs^+ produces a hole on the surface and enters the nanotube.

ring "β". All the second-nearest-neighbor atoms are called "γ". All the bonds between any pair of neighboring α and β atoms are called "$\alpha\beta$" bonds, while "$\beta\gamma$" indicates all the bonds between β and γ atoms. The distance between the Cs^+ and α and β atoms are indicated as "Cs−α" and "Cs−β", respectively. Figure 2 shows the details of the Cs^+ collision along the route **C3**(10,10).

4.1. Collision of Cs^+ at 100 eV along the Routes Aiming toward the Stems. The effective potential shown in Figure 2 is the sum of Hartree and exchange-correlation terms in Kohn−Sham Hamiltonian. Up to around 30 fs, the α atoms remain on the surface of the nanotube, and the effective potential increases due to reduction of Cs−α distances. After 30 fs, the α atoms are pushed inside the nanotube, and around 35 fs they become detached from the neighboring β atoms. This is evident from the minimum of the effective potential at 35 fs. At later times, both the Cs−α distances and $\alpha\beta$ bonds increase due to movement of the detached α carbon atoms inside the nanotube. Meanwhile, Cs−β distances decrease as Cs^+ gets closer to the nanotube; hence, there is continued increase of the effective potential.

Figure 3 exhibits the defect which is created by the Cs^+ collision along the route **C3**(10,10) with initial kinetic energy 100 eV at 55 fs. In this figure, a bond is drawn between two carbon atoms if their separation is less than 1.7 Å, which is about 20% more than the C−C equilibrium bond length 1.43 Å. The same rule is followed in all snapshot figures. In Figure 3, the Cs^+ is observed to be passing through the defect. Between 40 and 50 fs the distance between any pair of carbon atoms belonging to the hexagon ring, i.e, the α atoms, is determined

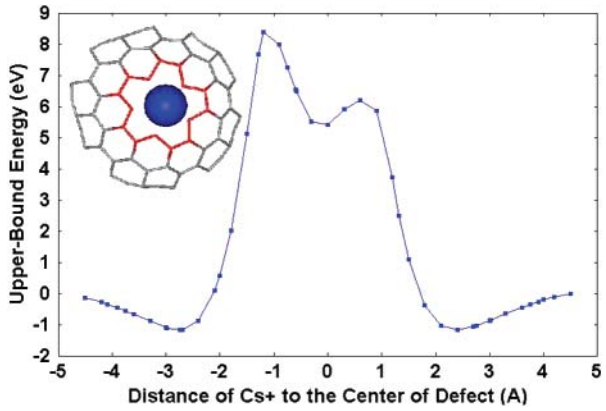

Figure 4. Upper bound for the energy barrier that Cs^+ faces upon entering the nanotube through the defect created along the route **C2**(10,10) (inset figure). Positive and negative distances indicate outside and inside of the nanotube, respectively.

to be more than 1.8 Å (the α bonds in Figure 2). It is true for all the $\alpha\beta$ bonds, too. This shows that between 40 and 50 fs the hexagon-ring atoms are shot toward inside of the nanotube as six individual carbon atoms. However at later times these individual atoms combine to make two carbon trimers as observed in Figure 3. The average of the C−C bond lengths in these trimers is 1.57 Å, and the average distance between nearest carbon atoms belonging to different trimer is 2.65 Å. Because of the existence of dangling bonds, these linear trimers are not stable and turn into two carbon triangles.

To calculate an upper bound for the potential barrier that Cs^+ faces while passing through the created defect, we perform a separate set of calculations. Upon the entering of Cs^+ into the nanotube along different routes, various defects are formed. The numbers of detached carbon atoms and diameters of the produced holes are different. We notice that the diameter of the hole produced via the **C2**(10,10) route is the smallest. This hole is created by detachment of a pentagon ring. We determine the detachment energy to be 45.0 eV. Our upper-bound calculations—as needed below—do not include this energy, as they concern the barrier that Cs^+ faces while passing through the *created* hole. For calculating the upper bound of barrier, we consider the **C2**(10,10) route. If the Cs^+ kinetic energy *after creating the hole* is bigger than the upper bond, then the Cs^+ will pass through the hole. The general features of the bond oscillations along the route **C2**(10,10) are similar to those along the route **C3**(10,10) depicted in Figure 2. In particular, the variations of the $\beta\gamma$ bond lengths are very small. Our calculations show that 96% of the kinetic energy which is transferred to the carbon lattice, when the distance between Cs^+ and the center of pentagon is 1.0 Å, is absorbed by the α (83%), β (10.2%), and γ (4.6%) carbon atoms. We therefore consider part of the carbon lattice including up to the 7th nearest neighbors of the collision site for upper-bound calculations. This portion of the nanotube includes 66 carbon atoms around the hole, with a diameter of 4.4 Å, produced by detachment of the pentagon (the pentagon itself is not included). The outermost bonds are saturated by reducing their lengths to 1.24 Å. The upper bound of the barrier, depicted in Figure 4, is calculated by fixing all the atoms for different distances between Cs^+ and the center of the hole and determining total potential energies. As in the actual collision the carbon atoms are free, using the fixed atoms mentioned above results in an upper bound for the barrier. In other words, the actual barrier height is shorter. As observed from Figure 4 the upper bound for the barrier is 8.4 eV. This means along any collision route that takes Cs^+ inside

BATCH: jp10b75 USER: dgw69 DIV: @xyv04/data1/CLS_pj/GRP_jp/JOB_i41/DIV_jp0481557 DATE: September 2, 2004

TABLE 2: Characteristics of Different Routes along Which Cs^+ Enters the Nanotube

route	diameter of the hole (Å)	effective potential (eV)	kinetic energy of the Cs^+ (eV)
C1(10,10)	4.6	42.0	11.2
C2(10,10)	4.5	43.6	9.9
C3(10,10)	5.8	34.5	22.9
S1(10,10)	5.1	31.2	29.7
S3(10,10)	4.9	38.6	29.3
S4(10,10)	5.8	41.3	20.8

the nanotube, if the kinetic energy of Cs^+ after creating the hole is bigger than 8.4 eV, then the Cs^+ will pass through the hole. Figure 4 shows that there are two local maxima at −1.3 and 0.9 Å with the maximum inside being more pronounced. There are three local minima at −2.7, 0.0, and 2.4 Å. The minimum at −2.7 Å is a little (∼0.1 eV) deeper than the minimum at 2.4 Å. These observations are attributed to the curvature of the tube. In the MD simulation, after the creation of the hole, the $\beta\gamma$ bond lengths are reduced to 1.34 Å. This shows that the nature of the bonding between β and γ atoms gets closer to double bond, which prevents the existence of dangling bonds within the surface of the nanotube. Therefore, the density of electrons at the center of the hole is less than the p electron densities outside and inside of the nanotube. This is the reason that we observe a minimum at the center of the hole.

In Table 2, we show the diameter of created hole, the effective potential, and the kinetic energy of Cs^+ when the distance of the Cs^+ from the starting point in MD simulation is 4.0 Å (the distance of the starting position of the Cs^+ to the target is 4.0 Å for all the routes along which the Cs^+ enters the nanotube). The sum of the effective potential, the kinetic energy of Cs^+, and the kinetic energy of the carbon atoms (not shown) is 100 eV. The diameter of the created hole is the diameter of the circle passing through the vertexes of the regular polygon whose side length is the average of the β bonds. Although the time steps at which the information in Table 2 is extracted are different for different routes, all the routes show the detachment of α atoms and the creation of the hole after Cs^+ has moved 4.0 Å away from its starting point. Taking into account that the upper bound of the potential barrier for Cs^+ insertion is 8.4 eV, and considering the kinetic energies of Cs^+ in Table 2, we conclude that the Cs^+ will enter the nanotube. However, the kinetic energies of Cs^+ after creating the hole along different routes are not enough for creating a second hole in the opposite side of the wall. Consequently, the Cs^+ will be encapsulated along all of the routes indicated in Table 2.

The diameters of the created hole along different routes depend on the empty space created by the detachment of the α carbon atoms. For example, the number of detached carbon atoms along the routes **C1**(10,10) and **S1**(10,10) is five and four, respectively. But the diameter of the created hole along the route **S1**(10,10) is larger than the one along the route **C1**(10,10). In Table 2, it is observed that the heights of the effective potential along different routes are different. This difference is caused by the difference in impact positions and the curvature of the tube, manifested through the necessary energy for detaching the α carbon atoms and the distance between the Cs^+ and the β atoms (Cs−β). If the numbers of the detached α atoms for two routes are the same, then the route with smaller hole diameter will have higher effective potential due to bigger repulsion between the Cs^+ and β atoms. This explains why the observed effective potentials along **C1**(10,10) is less than that of **C2**(10,10). However, if the numbers of the detached α atoms are different, then the required detachment energy will be the dominant factor and will overrule the effect of the hole diameter.

TABLE 3: Charactristics of Different Routes along Which Cs^+ Is Scattered off the Nanotube

route	no. of torn bonds	no. of detached atoms	kinetic energy of target carbon atom (eV)	scattering angle of Cs^+ (deg)	kinetic energy of Cs^+ (eV)
C4(10,10)	3	1	9.1	39.0	48.2
S2(10,10)	3	0	3.2	39.4	39.4

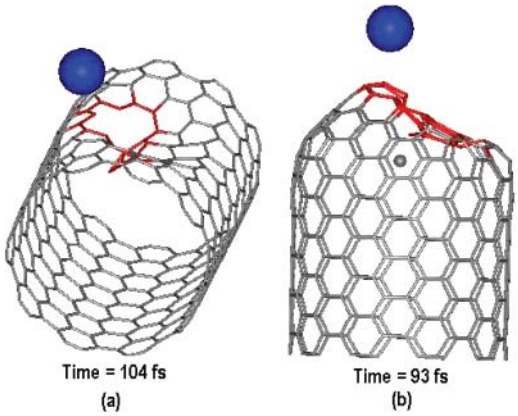

Figure 5. Snapshots of Cs^+ collision with the stem (a) and cap (b) of (10,10) nanotube along the routes **S2**(10,10) and **C4**(10,10) at 104 and 93 fs, respectively. Initial kinetic energy of Cs^+ is 100 eV. The Cs^+ scatters off the nanotube after tearing the wall.

This situation is seen, e.g., for the routes **S1**(10,10) and **C3**(10,10) where despite its smaller hole diameter, **S1**(10,10) has lower effective potential due to its less number of detached α atoms, as mentioned above. As another example we notice that although both the numbers of the detached α atoms and the hole diameters are the same along **S4**(10,10) and **C3**(10,10), the effective potential is much lower for **C3**(10,10) due to reduced coulomb repulsion between the Cs^+ and β atoms (bigger Cs−β bonds), resulting from cap's curvature.

4.2. Collision of Cs^+ at 100 eV along the Routes Aiming away from the Stems. In Table 3, we show the number of torn bonds (the bonds whose lengths are more than 1.7 Å), the number of detached atoms, the kinetic energy of target atom, scattering angle of the Cs^+ (the deviation angle of the scattering Cs^+ direction from the original route along which the Cs^+ approaches the target), and the kinetic energy of Cs^+ when the distance of Cs^+ from the starting point in MD simulation is 6.9 Å. At this distance the exerted force on the Cs^+ is less than 1.2 eV/Å. For both of the routes mentioned in Table 3, the Cs^+ has already torn off part of the nanotube surface. Curvature effects at the cap and stem of the nanotube are observed from the results mentioned in Table 3. Along the route **S2**(10,10) the Cs^+ interacts with more carbon atoms as compared with those along the route **C4**(10,10). Therefore, the transferred kinetic energy to the target atom (3.2 eV) is not enough for detachment of the target along **S2**(10,10). Figure 5a shows that the Cs^+ which is shot along the route **S2**(10,10) is going away from the nanotube after tearing its body. Along the route **C4**(10,10), the kinetic energy transferred from Cs^+ is concentrated on the target atom (9.1 eV). The target atom is therefore detached, as is observed from Figure 5b. Along both of the routes shown in Table 3 the force exerted by the carbon atoms causes the Cs^+ to scatter off the nanotube with an angle around 39.0° with respect to the original direction of approach. As a result of tearing part of the nanotube by the scattered Cs^+, it would be possible for a second Cs^+ to enter the nanotube via the torn region.

The general form of the produced holes during the collision of Cs^+ to the cap/stem of the (5,5) nanotube is like the case of

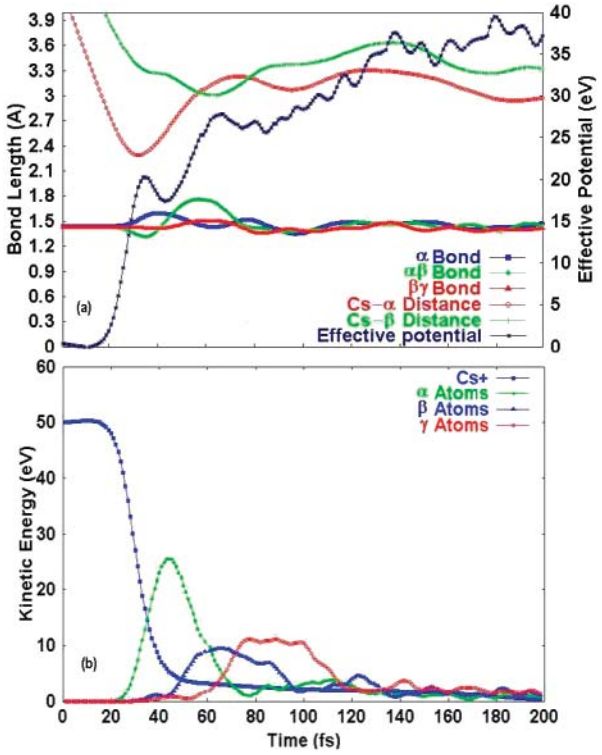

Figure 6. (a) Effective potential and the averages of the α, αβ, and $\beta\gamma$ bonds as well as the Cs−α and Cs−β distances vs time along the route **C3**(10,10). (b) Kinetic energy of Cs^+ together with that of all the α, β, and γ carbon atoms vs time along the route **C3**(10,10). The initial kinetic energy of Cs^+ is 50 eV.

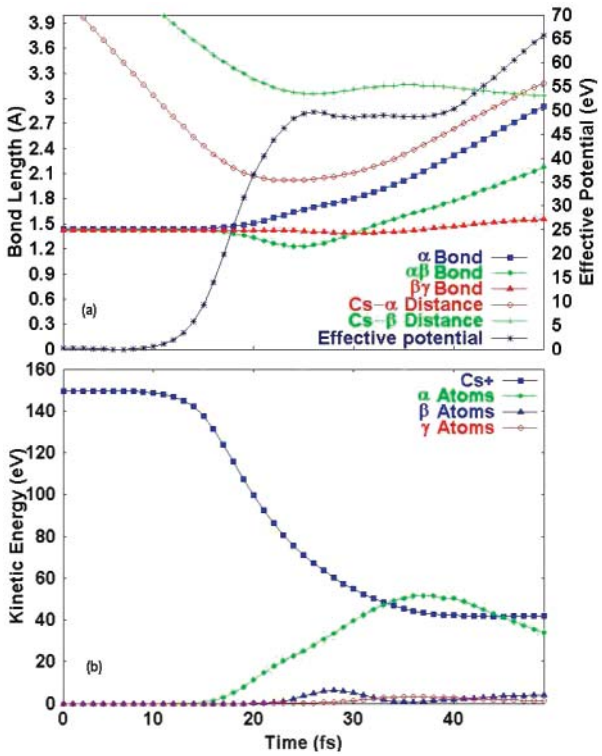

Figure 7. (a) Effective potential and the averages of the α, αβ, and $\beta\gamma$ bonds as well as the Cs−α and Cs−β distances vs time along the route **C3**(10,10). (b) Kinetic energy of Cs^+ together with that of all the α, β, and γ carbon atoms vs time along the route **C3**(10,10). The initial kinetic energy of Cs^+ is 150 eV.

the cap/stem of the (10,10) nanotube. Nevertheless, because of the smaller radius of (5,5) as compare to (10,10), complete encapsulation of the Cs^+ is not observed. Along some routes (**C2**(5,5), **S1**(5,5), and **C3**(5,5)), it is observed that the Cs^+ slightly enters the hole created by detachment of carbon atoms. The detached atoms create a bridgelike structure between the opposite sides of the nanotube wall in a local sp^3 bonding. These bridgelike structures block further progress of the Cs^+ inside the nanotube. When the Cs^+ is shot along the routes **C4**(5,5) and **S2**(5,5), it tears the nanotube and leaves its surface. The number of torn bonds is on the average twice as that of (10,10) case. However, for (5,5) the detached atoms are trapped as part of the bridgelike structure. As a result of smaller radius of (5,5) that leads to smaller number of carbon atoms interacting with the incoming Cs^+, the scattering angle for (5,5), ∼32.5°, is less than that of (10,10) (Table 3).

Although our discussions are based on Cs^+ collision, we checked that the results for neutral Cs collision were almost the same (with minor, ∼0.1 eV, difference in effective potentials). After collision the Mulliken charge of both Cs and Cs^+ is 0.6 e. The essential benefit of Cs^+ is its acceleration under electric field in actual experiments.[19,20]

4.3. Collision of Cs^+ at 50 eV. Next, we consider the Cs^+ collision with initial kinetic energy 50 eV. The Cs^+ is shot along all the routes mentioned in Table 2. Figure 6a,b shows the results along the route **C3**(10,10). From Figure 6a, it is observed that during the times between 55 and 65 fs the Cs^+ elongates the αβ bonds. However, at later times the αβ bonds restore their original length. Figure 6b indicates the kinetic energy of Cs^+ and the transferred kinetic energy to the α, β, and γ atoms. It is observed that the Cs^+ collision causes a distortion wave that is defusing to the whole system. The corresponding oscillations of the carbon lattice are responsible for the observed small maxima and minima in effective potential curve in Figure 6a. Figure 6b also shows that the kinetic energy of the Cs^+ decreases to 0.0 eV. Therefore, the Cs^+ cannot break any of the C−C bonds and cannot enter the nanotube. It is worth mentioning that 50 eV collision along the route **S1**(10,10) (not shown in the figures) indicates a faster propagation of the distortion wave such that after 134 fs it moves 8.0 Å away from the impact point. This should be compared with the **C3**(10,10) results depicted in Figure 6a,b, that indicates slower propagation of the distortion wave.

4.4. Collision of Cs^+ at 150 eV. As we observed, the Cs^+ with initial kinetic energy 100 eV was encapsulated along the routes mentioned in Table 2. Therefore, we expect that the Cs^+ with higher kinetic energy can be encapsulated at least along the same routes. To consider the effects of higher kinetic energies, the Cs^+ is shot along the route **C3**(10,10) with initial kinetic energy 150 eV. The results are depicted in Figure 7a,b. Figure 7a shows that at 40 fs both the α and αβ bonds are broken (the bond lengths are more than 1.7 Å); it is an indication that the detached α atoms are separated from each other and are shot toward the inside of the nanotube as six individual "runaway" carbon atoms. These individual atoms are not stable and presumably combine with each other, or with individual carbon atoms resulting from other similar collisions, to form carbon dimers or trimer triangles at a later time. As with the initial impact energy 150 eV the carbon atoms have less time for relaxation, the height of the observed effective potential at 150 eV (Figure 7a) is more than the corresponding height at 100 eV (Figure 2). Figure 7b indicates the kinetic energy of Cs^+ and the transferred kinetic energies to the α, β, and γ atoms. It shows that the kinetic energies transferred to β and γ atoms are much less than that transferred to the α atoms. Therefore, the deformed area for high-energy impact is smaller than the

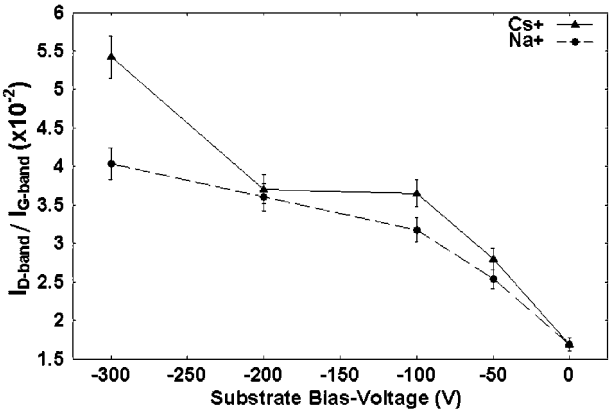

Figure 8. Variation of intensity ratio (I_D/I_G) of the Raman peaks with the absolute value of substrate bias voltage.

deformed area at low-energy impact. It is further observed that the kinetic energy of Cs^+ is nearly constant after entering the tube. However, this energy is not enough for passing through the other side, and the Cs^+ is encapsulated. The Cs^+ and runaway α carbon atoms can make a distortion on the other side of the nanotube, without bond breaking. Subsequently, the runaway α atoms either leave the nanotube—through the hexagons of the nanotube wall—or get attached to the lattice in a local sp^3 structure.

4.5. Experiment. Next we consider the implications of our ab initio MD results in interpreting the experimental observations. Raman scattering spectroscopy has been adopted in order to evaluate the degree of structural deformation because defect-induced band (D-band) is associated with symmetry-lowering factors in disordered graphite. Therefore, peak intensity of the D-band (I_D) is sensitive to the amount of disorder in carbon nanotubes such as amorphous carbon, graphitic nanoclusters, or other defects. On the other hand, the graphite band (G-band) intensity (I_G) is related to graphite dispersion of the nanotube and characterized by peak splitting which is different from the spectrum of planar graphite.[35] For this reason, to estimate the deformed nanotube structures quantitatively in relation to the applied bias voltages, we introduce an intensity comparison of Raman peaks (I_D/I_G) as a quantitative barometer of the completeness of the single wall nanotube structure.

Figure 8 gives the relationship between the value of I_D/I_G and applied substrate bias voltage. From this result, it is found that the value of I_D/I_G increases with increasing the applied bias voltage value. In other words, the disordered nanostructures induced by tube cutting and bending increases due to increasing ion irradiation energy. The other interesting point is that the Cs^+ is more effective than Na^+ for the tube deformation. We therefore conjecture that the defect formation in our experiments is mainly caused by momentum transfer from the accelerated charged particles to the nanotubes.[20] The presence of a plateau between 100 and 200 V in the Cs^+ results and the absence of such behavior in Na^+ results are worth noticing. As we saw, at 100 and 150 eV energies, the kinetic energy of Cs^+ after making the first hole in the nanotube's wall is reduced to ∼20−40 eV. This energy is not enough for making a hole in the other side of the wall, and Cs^+ is encapsulated. In other words, by increasing the bias voltage from 100 to 200 V, no essentially new defect is created, and the intensity ratio (I_D/I_G) remains practically constant. The radii of Na^+ and Cs^+ are around 1.0 and 1.7 Å, respectively. Therefore, Na^+ can make new defects on the other side of the wall, after entering the tube, and the intensity ratio increases for the Na^+ case.

5. Conclusions

In conclusion, we study the dynamical criteria in Cs^+ insertion and adsorption in carbon nanotubes by ab initio molecular dynamics (MD). Considering the three relevant factors of collision, that is impact angle (the routes aiming away from the stem and the routes aiming toward the stem), impact position (atom, bond, and the center of pentagon and hexagon rings), and the Cs^+ kinetic energy (50, 100, and 150 eV), it is observed that the Cs^+ with initial kinetic energy 100 and 150 eV can be encapsulated directly by making a hole on the surface or indirectly through the torn region resulting from a previously scattered Cs^+. Cs^+ encapsulation, which is further supported by Raman scattering spectroscopy, is useful in making nano-junctions in agreement with experimental results with potential application in nanoelectronics. The energy transfer rate to the highly curved regions of the nanotube (i.e., at the cap) is seen to be lower than the corresponding rate in collision with the stem. At high kinetic energies (100 and 150 eV), our calculations show that the Cs^+ transfers more than 70% of its kinetic energy to the carbon atoms at the impact position. Therefore, the carbon atoms at the impact position are detached from the nanotube. The detached carbon atoms which are not able to escape from inside of the tube get attached to the opposite side of the nanotube wall in a local sp^3 structure. At low kinetic energy, i.e., 50 eV, the whole energy of Cs^+ is transferred to the carbon lattice. The created distortion wave diffuses to the whole system. Hence, the deformation at 50 eV, although being temporarily larger in extent than those of 100 and 150 eV, is remedied, and the Cs^+ remains adsorbed on the tube. The adsorbed Cs^+ makes a sharp point on the surface that is convenient for field emission.

Acknowledgment. The authors sincerely thank the crew of the Center for Computational Materials Science of the Institute for Materials Reasearch, Tohoku University, for their countinuous support of the supercomputing facilities. This work is supported by the Special Coordination Funds of the Ministry of Education, Culture, Sports, Science and Technology of the Japanese government.

References and Notes

(1) Fan, S.; Chapline, M. G.; Franklin, N. R.; Tombler, T. W.; Cassell, A. M.; Dai, H. *Science* **1999**, *283*, 512.

(2) de Heer, W. A.; Chatelain, A.; Ugrate, D. *Science* **1995**, *270*, 1179.

(3) Wang, Q. H.; Setlur, A. A.; Lauerhaas, J. M.; Dai, J. Y.; Seelig, E. W.; Chang, R. P. H. *Appl. Phys. Lett.* **1998**, *72*, 2912.

(4) Kim, C.; Kim, B.; Lee, S. M.; Jo, C.; Lee, Y. H. *Phys. Rev. B* **2002**, *65*, 165418.

(5) Maiti, A.; Brabec, C. J.; Roland, C. M.; Bernholc, J. *Phys. Rev. Lett.* **1994**, *73*, 2468.

(6) Maiti, A.; Andzelm, J.; Tanpipat, N.; von Allmen, P. *Phys. Rev. Lett.* **2001**, *87*, 155502.

(7) Wadhawan, A.; Stallcup, R. E., II; Stephens, K. F., II; Perez, J. M.; Akwani, I. A. *Appl. Phys. Lett.* **2001**, *79*, 1867.

(8) Kim, C.; Seo, K.; Kim, B.; Park, N.; Choi, Y. S.; Park, K. A.; Lee, Y. H. *Phys. Rev. B* **2003**, *68*, 115403.

(9) *Physics and Chemistry of Alkali Metal Adsorption*; Bonzel, H. P., Bradshaw, A. M., Ertl, G., Eds.; Elsevier: Amsterdam, 1989.

(10) Pati, R.; Zhang, Y.; Nayak, S. K.; Ajayan, P. M. *Appl. Phys. Lett.* **2002**, *81*, 2638.

(11) Binh, V. T.; Purcell, S. T.; Garcia, N.; Doglioni, J. *Phys. Rev. Lett.* **1992**, *69*, 2527.

(12) Suzuki, S.; Bower, C.; Watanabe, Y.; Zhou, O. *Appl. Phys. Lett.* **2000**, *76*, 4007.

(13) Wadhawan, A.; Stallcup, R. E., II; Perez, J. M. *Appl. Phys. Lett.* **2001**, *78*, 108.

(14) Zhao, J.; Han, J.; Lu, J. P. *Phys. Rev. B* **2002**, *65*, 193401.

(15) Esfarjani, K.; Farajian, A. A.; Hashi, Y.; Kawazoe, Y. *Appl. Phys. Lett.* **1999**, *74*, 79.

(16) Farajian, A. A.; Esfarjani, K.; Kawazoe, Y. *Phys. Rev. Lett.* **1999**, *82*, 5084.
(17) Shimoda, H.; Gao, B.; Tang, X. P.; Kleinhammes, A.; Fleming, L.; Wu, Y.; Zhou, O. *Phys. Rev. Lett.* **2002**, *88*, 015502.
(18) Liu, X.; Pichler, T.; Knupfer, M.; Fink, J. *Phys. Rev. B* **2003**, *67*, 125403.
(19) Jeong, G.-H.; Farajian, A. A.; Hirata, T.; Hatakeyama, R.; Tohji, K.; Briere, T. M.; Mizuseki, H.; Kawazoe, Y. *Thin Solid Films* **2003**, *435*, 307.
(20) Jeong, G.-H.; Farajian, A. A.; Hatakeyama, R.; Yaguchi, T.; Tohji, K.; Mizuseki, H.; Kawazoe, Y. *Phys. Rev. B* **2003**, *68*, 075410.
(21) Although it is believed that single wall nanotubes stand aligned parallel to the electric field, the sea urchin nanotubes are nevertheless distributed randomly.
(22) Farajian, A. A.; Ohno, K.; Esfarjani, K.; Maruyama, Y.; Kawazoe, Y. *J. Chem. Phys.* **1999**, *111*, 2164.
(23) Mann, D. J.; Halls, M. D. *J. Chem. Phys.* **2002**, *116*, 9014.
(24) Park, N.; Han, S.; Ihm, J. *Phys. Rev. B* **2001**, *64*, 125401.
(25) Perdew, J. P.; Burke, K.; Ernzerhof, M. *Phys. Rev. Lett.* **1996**, *77*, 3865.
(26) Troullier, N.; Martins, J. L. *Phys. Rev. B* **1991**, *43*, 8861.
(27) Sankey, O. F.; Niklewski, D. J. *Phys. Rev. B* **1989**, *40*, 3979.
(28) Ordejon, P.; Artacho, E.; Soler, J. M. *Phys. Rev. B* **1996**, *53*, 10 441.
(29) Soler, J. M.; Artacho, E.; Gale, J. D.; Garcia, A.; Junquera, J.; Ordejon, P.; Sanchez-Portal, D. *J. Phys.: Condens. Matter* **2002**, *14*, 2745.
(30) Sachez-Portal, D.; Artacho, E.; Soler, J. M.; Rubio, A.; Ordejon, P. *Phys. Rev. B* **1999**, *59*, 12678.
(31) Sanchez-Portal, D.; Arracho, E.; Soler, J. M. *J. Phys.: Condens. Matter* **1996**, *8*, 3859.
(32) Moullet, I.; Andreoni, W.; Giannozzi, P. *J. Chem. Phys.* **1989**, *90*, 7306.
(33) Dreuw, A.; Cederbaum, L. S. *J. Chem. Phys.* **1999**, *111*, 1467.
(34) DiVincenzo, D. P.; Mele, E. J. *Phys. Rev. B* **1985**, *32*, 2538.
(35) Saito, R., Dresselhaus, G., Dresselhaus, M. S. *Physical Properties of Carbon Nanotubes*; Imperial College Press: London, 1998; p 187.